Laser cutting assisted fabrication of assembled solid-state supercapacitors based on polypyrrole coated paper

Ruirong Zhang[1,*], Sheng Cai[1], Qi Wu[1],Yao Zhu[1], Xu Yin[1], Yanmeng Xu[2], Yang Yang[3] and Honglong Chang[1,*]

1 Ministry of Education Key Laboratory of Micro/Nano Systems for Aerospace, School of Mechanical Engineering, Northwestern Polytechnical University, Xi'an 710072, China

2 Cleaner Electronics Group, College of Engineering, Design and Physical Sciences, Brunel University London, Uxbridge, UK

3 Ministry of Education Key Laboratory of Low-grade Energy Utilization Technologies and Systems, Chongqing University, Chongqing 400030, China

[*]E-mail: ruirongzhang@nwpu.edu.cn; changhl@nwpu.edu.cn

Abstract

In this work, a simple process has been demonstrated to fabricate solid-state paper-based supercapacitors. A highly conductive paper was prepared through coating polypyrrole on cellulose paper by interfacial polymerization. Among the PPy/paper samples prepared using different Py concentrations of 0.5%, 1.0%, 2.0% and 2.5%, PPy/paper (1.0% Py) displayed the best electrochemical performance (445.3 mF cm^{-2} and 247.4 F/g at 0.01 V s^{-1}) and a good flexibility: the conductivity could retain near the original value even after being bent 450 times. Then, the PPy/paper (1.0% Py) electrodes with desired shapes were manufactured easily by laser cutting. A thin solid-state planar supercapacitor unit was fabricated by assembling the two PPy/paper electrodes and polyvinyl alcohol/H_3PO_4 electrolyte, and it exhibited a capacity of 51.6 mF and a high areal specific capacitance of 12.9 mF cm^{-2}. Furthermore, 8 supercapacitor units were connected in series and parallel to obtain a thin supercapacitor array generating a higher output voltage and capacity. The

supercapacitor array was integrated with a flexible printed circuit board, and it lighted up 3 light-emitting diodes, even under bending conditions. This method can be used to scale up the fabrication of flexible integrated paper-based energy storage devices for various portable and wearable electronics.

Key words: Paper-based supercapacitor; Solid-state; Flexible; Laser cutting; PPy/paper

1. Introduction

The rapid increasing consumption of personal electronics and development of portable/wearable electronic devices has greatly promoted the development of matching flexible power sources [1-4]. Because of processing high power density, fast charge/discharge rates, long life cycle and being environmentally friendly and long cycle life, flexible supercapacitors have attracted much attention in the field of flexible power sources [5-7]. The electrode substrate plays an important role in the flexible supercapacitors. With the advantages of being cheap, lightweight, flexible, environmentally friendly and biodegradable, the normal printing paper has recently been considered as a potential substrate for flexible supercapacitors [8-12]. Cui et al. designed and fabricated supercapacitors by directly drawing graphite on cellulose paper [13]. The porous paper served as a flexible substrate and also an excellent separator in this supercapacitor. This paper-based supercapacitor showed a stable long cycling performance and a high areal capacitance of 2.3 mF cm^{-2}. It was worth noting that this supercapacitor was sealed in a polymer bag to form a pouch cell because the aqueous electrolyte (1 M H_2SO_4) was used. Furthermore, Down et al. produced a paper-based supercapacitor with an interdigitated structure by commercial pencils drawing upon common printing paper [14]. This device utilizing PVA/H_2SO_4 gel electrolyte demonstrated a specific capacitance of 141.8 μF g^{-1} at a charging current of 4.33 μA g^{-1}. Compared with liquid flexible supercapacitors, this kind of solid-state paper supercapacitors possess a series of attractive features, such as lightweight, high safety and high flexibility, and were considered to be the effective device for portable and wearable electronics [15-18]. The above paper-based supercapacitors were fabricated using a simple and economical drawing method. Because the pencil 'lead' consists of a mixture of graphite, wax and clay, the limited mass of graphite could be coated on the

paper. Moreover, the paper-based supercapacitors utilizing carbon materials, such as graphite, usually exhibit a limited specific capacitance due to the electric double layer storage mechanism of carbon-based materials [12-14, 19]. The limited specific capacitance further results in a limited energy density, which is a major challenge to commercialize this flexible paper supercapacitors for real-time applications. Therefore, it is critical to fabricate a paper supercapacitor with high electrochemical performance by facile methods.

In general, pseudocapacitive materials, such as metal oxide and conducting polymers, have a much higher specific capacitance compared with the carbon materials [20,21]. Among them, polypyrrole (PPy) is considered as a promising candidate because of its high conductivity, good environmental stability, ultrahigh-flexibility and easy preparation. Meantime, there are abundant nitrogen atoms in the pyrrole ring, which are beneficial to enhance the hydrophilicity of the electrode materials. The hydrophilicity of the electrode materials can remarkably improve the wettability of the electrodes, then significantly promote electrolyte ions diffusion and improve the ion-accessible surface area [22]. Chen et al. coated PPy onto air-laid paper by an interfacial polymerization method to fabricate flexible solid-state supercapacitors. The prepared sandwiched PPy-coated paper-based supercapacitors exhibited a high energy density and an excellent flexibility [22]. The interfacial polymerization method to prepare PPy is simple, facile, efficient and can be easily scaled up for production of paper electrode. Moreover, the above sandwich structure is a typical configuration of supercapacitor, which comprises two electrodes face-to-face with a separator between them. The other typical configuration is a planar structure of two electrodes in-plane supercapacitor, which can significantly decrease the thickness in the vertical direction to achieve thin and flexible devices and shows more capacity in miniaturization and a potential for integration with

on-chip electronics [23]. However, there are few reports focused on the paper-based supercapacitors with two electrodes in-plane type. The main challenge is to develop a simple process to manufacture the planar paper-based electrodes.

Recently, the laser cutting technique has been used as a simple fabrication method to obtain paper engraving with various structures, which can be applied on programmable patterning on arbitrary substrates with high resolution. Therefore, the laser cutting was also considered as a versatile method to fabricate other paper-based devices [23,24]. Inspired by the above work, the simple laser cutting method was adopted in this research work to shape PPy coated paper (PPy/paper) based electrodes for supercapacitors in this work. The PPy/paper was prepared by a chemical interfacial polymerization process. The optimized PPy/paper showed a high specific capacitance of 445.3 mF cm^{-2}, a good hydrophilicity and a good flexibility. A solid-state supercapacitor unit with PPy/paper electrodes shaped by CO_2 laser cutting showed a high areal specific capacitance of 12.9 mF cm^{-2}. Then, 8 supercapacitor units were integrated with flexible printed circuit board (FPCB), which lighted up 3 light-emitting diodes (LEDs) even under bending conditions. The demonstrated process developed a novel manufacturing method for the fabrication of flexible solid-state planar paper-based supercapacitors, which could be a potential power supply to various portable and wearable electronics.

2. Experimental

2.1 Materials and reagents

Common printing paper from Deli Group Co. (Zhejiang, China) was selected. Pyrrole (Py, 98%), Cyclohexane, iron (Ⅲ) chloride, polyvinyl alcohol (PVA, average Mw

85000-124000, 87-89% hydrolyzed) and hydrochloric acid were supplied by Adamas Co. (Shanghai, China) and directly used without further purification. In addition, anhydrous ethanol from Greagent Co. (Shanghai, China) was chosen, and phosphoric acid was supplied by J&K Scientific Co. (Beijing, China).

2.2 Preparation of PPy/paper

PPy/paper with good flexibility and loose structure was produced by using the interfacial polymerization method (Fig. 1a). Firstly, the printing paper was immersed into 1 M hydrochloric acid and then deionized water (DI water) repeatedly to remove whitening agent between the cellulose fibers in the printing paper. The acid-treated paper was then placed and dried in a fume hood. In the next step, $FeCl_3$ was dissolved in the DI water with 9.2% mass ratio and 0.3 M hydrochloric acid was added to prevent the hydrolysis of $FeCl_3$, the obtained aqueous solution was poured into a round vessel (150 mm diameter), while the pyrrole was dissolved in the organic solvent cyclohexane with 1.0% volume ratio. Then, the acid-treated paper (80×80 mm^2) was immersed in a ferric chloride solution containing hydrochloric, the pyrrole monomer in cyclohexane (20 mL) was slowly dripped into the vessel. As the two phases contacted, the pyrrole monomers were oxidized and then polymerized on the surface of the cellulose fibers to form PPy. The whole reaction process was performed statically for 8 h. It should be worth noting that, the appropriately excessive oxidant ($FeCl_3$) and a long enough reaction time are necessary to ensure a sufficiently processed interfacial polymerization. After polymerization, PPy/paper was taken out and washed by deionized water and ethanol alternately, and subsequently PPy/paper was dried in a heating oven at 40 ℃ for 1 h, then placed in a fume hood to dry it. Four different samples, marked PPy/paper (0.5% Py), PPy/paper (1.0% Py), PPy/paper (2.0% Py) and

PPy/paper (2.5% Py), were prepared by using different pyrrole solutions with the pyrrole concentration of 0.5%, 1.0%, 2.0% and 2.5%, respectively.

2.3 Fabrication of paper-based supercapacitors

As shown in Fig. 1b, the PPy/paper was quickly and accurately cut into complementary shapes as electrodes by using the nonmetal cutting and engraving machine with CO_2 laser (E1309, cutting power: 8-10 W, cutting speed: 260-350 m/min), which was produced by Zhengtian Co. (Beijing, China). The PVA/H_3PO_4 gel electrolyte was fabricated by stirring 2 g of PVA powder and 3.92 g of phosphoric acid with 20 mL DI water at 80 ℃ for 1 h. The two electrodes with complementary shapes were fixed together on a plastic film and the gel electrolyte was coated onto the two electrodes and the gap between them. Then the device was left in a fume hood at room temperature to vaporize the extra water.

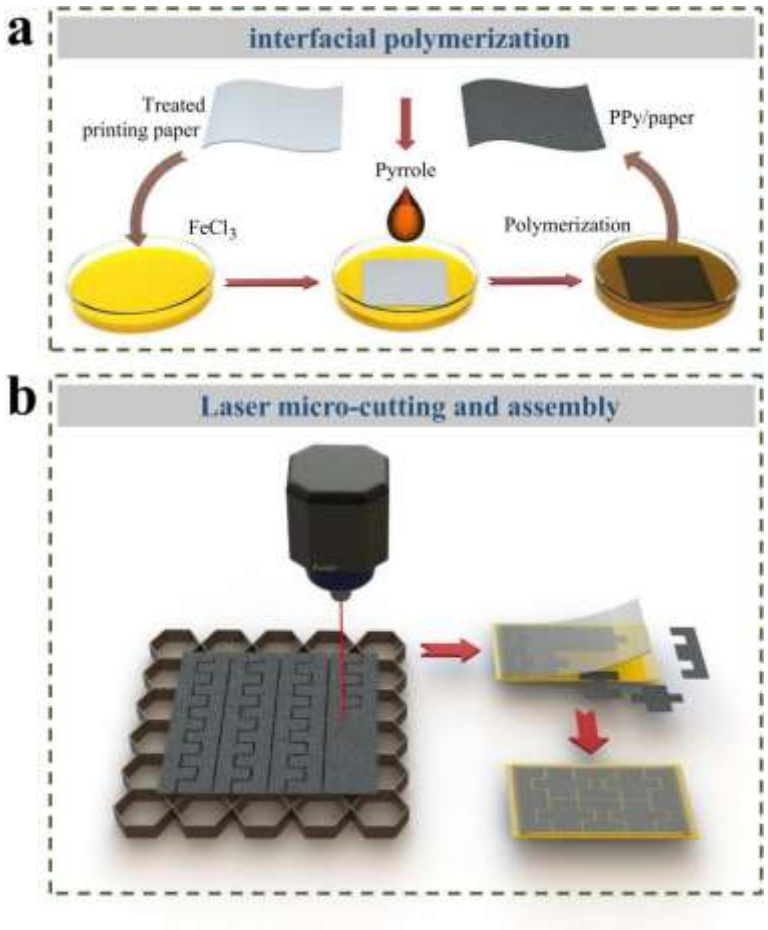

Fig. 1. (a) Schematic diagram of the fabrication of PPy/paper; (b) Schematic diagram of the fabrication of the electrodes by laser cutting and the assembly of array of electrodes with gel electrolyte.

2.4 Characterization methods and tools

The morphology of samples was characterized by a high-resolution field emission scanning electron microscope (FE-SEM, SU8020). The structure of the samples was characterized by Fourier transform infrared spectra (FT-IR) on a Nicolet IS10 spectrometer. The electrochemical measurements were carried out at room temperature using CHI 660E (CH Instrument). The characterization test was carried out in a three-electrode system. A piece of PPy/paper immersed in 2 M phosphoric acid served as the working electrode, a Pt sheet, and a saturated calomel electrode (SCE) worked as

counter electrode and reference electrode, respectively. The electrochemical impedance spectroscopy (EIS) was recorded in a frequency range from 100 kHz to 0.01 Hz with a potential amplitude of 5 mV.

The specific capacitance (C_m) and areal specific capacitance of the single electrode (C_A) was calculated from cyclic voltammetry (CV) and galvanostatic charge-discharge (GCD) curves based on the following equations:

$$C_m = \frac{Q_{total}/2}{\Delta U \times m_{ele}} \quad (1)$$

$$C_m = \frac{I\Delta t}{\Delta U \times m_{ele}} \quad (2)$$

$$C_A = \frac{Q_{total}/2}{\Delta U \times A_{ele}} \quad (3)$$

$$C_A = \frac{I\Delta t}{\Delta U \times A_{ele}} \quad (4)$$

where Q_{total} is the total charge moved inside the i-V loop, ΔU is the potential range, I represents the discharging current of GCD, Δt stands for the discharge time and m_{ele} is the mass of PPy/paper electrode, and A_{ele} is the area of the PPy/paper electrode.

The electrochemical performance of the assembled paper-based supercapacitor was tested via a two-electrode system. The area specific capacitance ($C_{A,device}$) of the device was obtained from the CV curve using the following equation:

$$C_{A,device} = \frac{Q_{total}/2}{\Delta U \times A_{device}} \quad (5)$$

where Q_{total} is the total charge moved inside the i-V loop with a scan range of ΔU, the A_{device} is the area of the whole device including the electrodes and the gel electrolyte.

The areal energy density of the device (E_A) was calculated from the equation:

$$E_A = \frac{C_{A,device} \times \Delta U^2}{2 \times 3600} \quad (6)$$

$C_{A,device}$ is the areal specific capacitance calculated from equation (5), and ΔU is the potential range.

3 Results and discussion

The fabrication processes of PPy/paper and solid-state paper-based supercapacitors have schematically illustrated in Fig. 1. The practical fabrication steps of PPy/paper are shown in Fig. 2a-c in corresponding to Fig. 1a. The acid-treated paper was immersed in ferric chloride solution containing hydrochloric as shown in Fig 2a; the pyrrole monomer in cyclohexane was added slowly to the ferric chloride solution, then the white paper turned to black gradually, Fig. 2b; after reacting for 8 h, the whole paper turned to black, demonstrating the paper was coated with PPy as shown in Fig. 2c. Fig. 2d shows the comparison of the printing paper before and after PPy coating, where the inset demonstrates the flexibility of the coated paper retained under the severe rolling condition. The detailed morphologies of the printing paper, acid-treated paper and PPy/paper at different magnifications were characterized by SEM as shown in Fig S1 (Supplementary Figures) and Fig. 2e-g. As shown in Fig. S1, the whitening agent with calcium carbonate as the main component [25] generally exists in the gap of the cellulose fibers of the printing paper. After the treatment of hydrochloric acid and deionized water, the cellulose fibers are still obvious, while the whitening agent is disappearing in the acid-treated paper, Fig. 2e-f. It can be observed that the porous structure of cellulose paper was still remained after PPy coating, Fig. 2h-j. The roughness of the cellulose fibers in the PPy/paper (Fig. 2j) increased compared with

that in acid-treated paper (Fig. 2g) due to the growth of polymer on the cellulose fibers as a consequence of the polymerization process, which presents some spherical small polymeric particles with an average diameter of about 29 nm, resulting in the fine electrical conductivity of the PPy/paper. The numerous micro/nano pores in the PPy/paper will be beneficial to the transport of the electrolyte (Fig. 2h-j) and thus facilitate the diffusion of electrolyte ions.

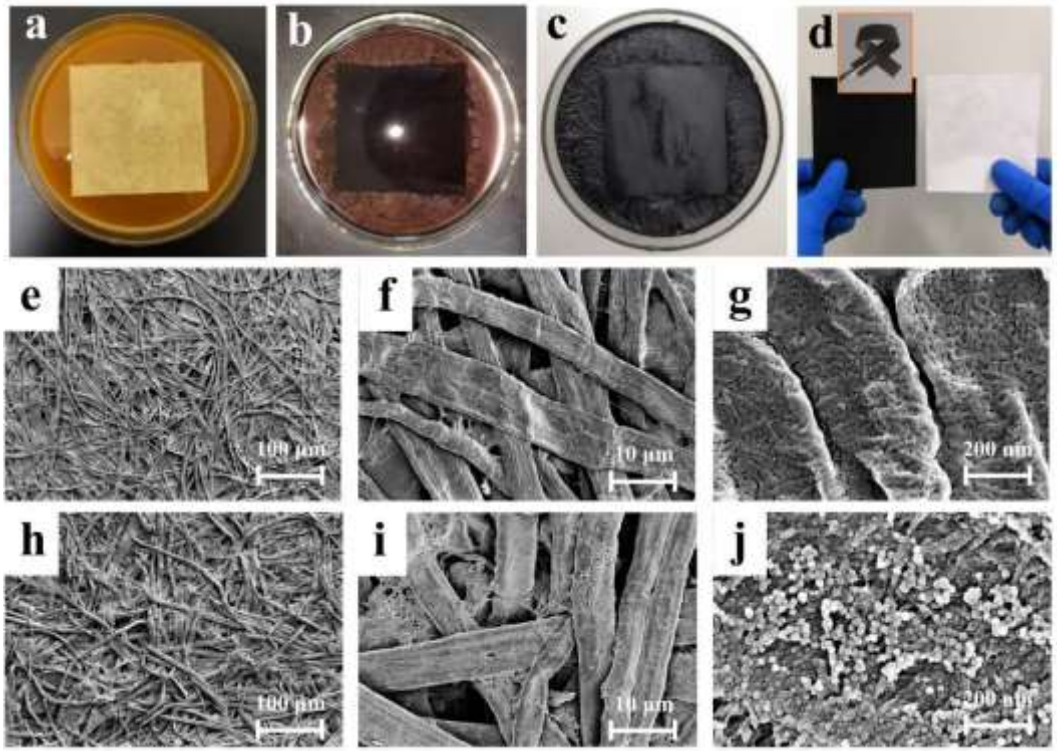

Fig. 2. (a-c) Optical pictures of the fabrication process of PPy/paper by interfacial polymerization; (d) Comparison of PPy/paper and printing paper, the inset shows the picture of PPy/paper in bending state; (e-g) SEM images of acid-treated paper at different magnifications; (h-j) SEM images of PPy/paper at different magnifications.

The chemical composition of the printing paper before and after interfacial polymerization of PPy were analyzed by FT-IR and the result is shown in Fig. 3. As shown in the spectra of the printing paper, the characteristic broad band for the O-H

group appears around 3329 cm^{-1} and the characteristic peak near 2897 cm^{-1}, which is related to the asymmetrically stretching vibration of C-H [26]. Furthermore, the broad absorption band between 1200 cm^{-1} to 900 cm^{-1} corresponds to various functional groups such as C-O and C-O-C. Compared with the spectra of the printing paper, the FT-IR spectrum of PPy/paper mainly presents the characteristic peaks of PPy. Specifically, the absorption peaks at 1642, 1081, and 997 cm^{-1} might be attributed to the C=C and C-C in-ring-stretching, and C-H out-of-plane deformation vibration, respectively [27]. In addition, the C-N stretching vibration absorption peaks on the pyrrole ring of the PPy appear at 1526 cm^{-1} and 1284 cm^{-1} [28]. These characteristic signals indicate that the PPy has successfully been coated on the printing paper.

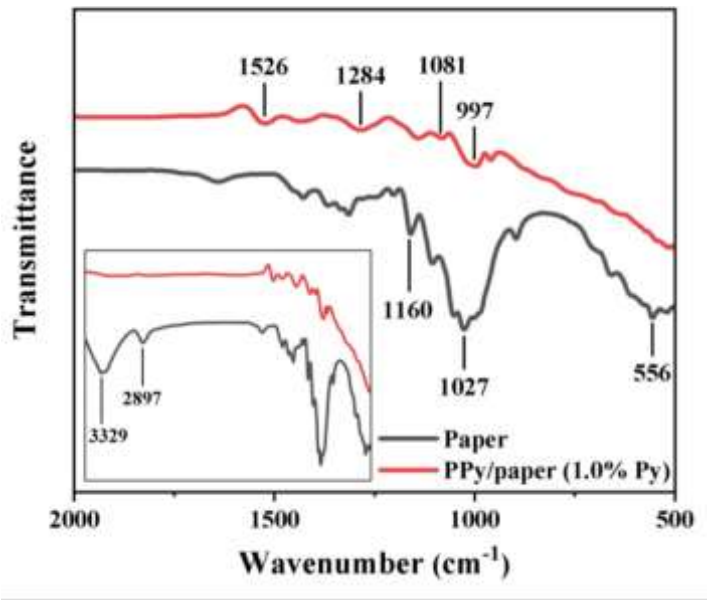

Fig. 3. FT-IR spectra of printing paper and PPy/paper (1.0% Py).

The wettability of the printing paper, acid-treated paper and PPy/paper samples fabricated with Py concentration of 0.5%, 1.0%, 2.0% and 2.5% were studied by the dynamic water contact angle measurement, and the results are shown in Fig. 4 and Fig. S2 (Supplementary Figures). The contact angles of PPy/paper samples fabricated with different Py concentrations (0.5%, 1.0%, 2.0% and 2.5%) are 85.4°, 30°, 52.9° and

61.7°, which are smaller than that of the printing paper (103.2°) or acid-treated paper (90.5°), indicating that the hydrophilicity of paper was improved after being coated by PPy. The reason is that the surface of PPy/paper exhibits homogeneous submicron scale spherical PPy particles on the cellulose fibers, which improved the hydrophilicity [29].

Furthermore, it is obvious that PPy/paper (1.0% Py) displays the smallest contact angle among the four PPy/paper samples prepared with different pyrrole concentration. As the increase of Py concentration from 0.5% to 1.0%, more PPy was attached to the surface of cellulose fibers, forming more hydrogen bonds, resulting in a rougher surface so it improves its hydrophilicity. However, as the Py concentration continued to increase, the PPy covered on the cellulose fibers became thicker and more compact, which would affect the porous network structure of cellulose fibers [30]. As a result, the surface tension of the water droplet prevents it from entering the PPy/paper with a compact PPy layer, resulting in lager contact angles, which means a lower hydrophilicity. This PPy/paper (1.0% Py) exhibits the best hydrophilicity in this work, which improved the wettability and could promote the diffusion of electrolyte ions [22].

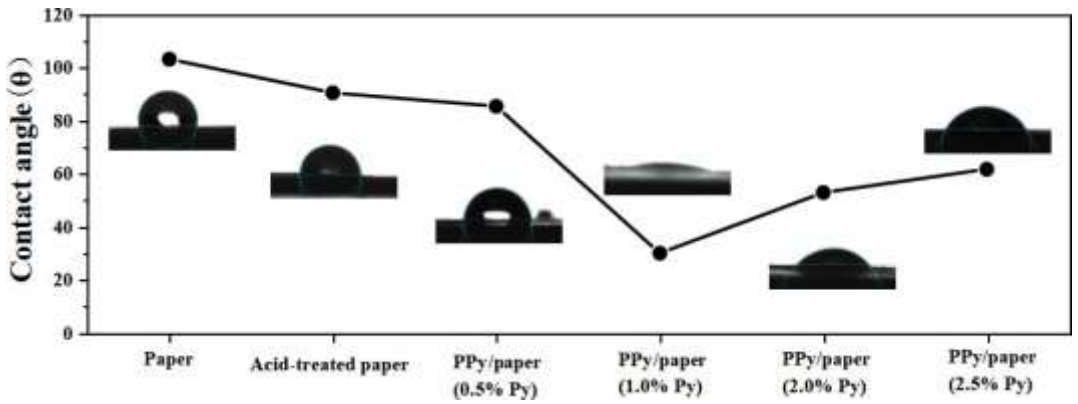

Fig. 4. Contact angles of the original printing paper, acid-treated paper and PPy/paper fabricated with different Py concentrations.

In order to evaluate the electrochemical performance of the PPy/paper electrodes prepared with different Py concentrations (0.5%, 1.0%, 2.0% and 2.5%), CV tests were performed in a three-electrode system in 2 M H_3PO_4 aqueous electrolyte at room temperature. Fig. 5a-d exhibit the CV curves of the PPy/paper samples fabricated with different Py concentrations (0.5%, 1.0%, 2.0% and 2.5%) at the scan rates of 0.01 V s^{-1}, 0.02 V s^{-1}, 0.04 V s^{-1} and 0.08 V s^{-1} under the potential window of 0-0.8 V. It can be seen that the CV curves of four PPy/paper samples are similar and they are different from the ideal rectangular shape for double-layer capacitance, which indicates the existence of the pseudocapacitance of the PPy/paper electrode. It can be noted that the charge current increases with the scan rate increasing simultaneously, while the shapes of the CV curves of the four PPy/paper samples have no obvious change at different scan rates as shown in Fig. 5a-d. That indicates a stable electrochemical property of the four PPy/paper samples. Based on the CV curves, the specific capacitance and areal specific capacitance of the PPy/paper samples were calculated and the values were plotted in Fig. 5e. It is worth noting that the PPy/paper (1.0% Py) electrode maintains the highest specific capacitance among the four samples under the CV test at different scan rates, indicating a better electrochemical performance. When the Py concentration increases from 0.5% to 1.0%, the specific capacitance increased from 106.6 F/g to 247.4 F/g at a scan rate of 0.01V/s, then when the Py concentration increased to 2.0% or 2.5%, PPy continuously covered on the cellulose fibers to form a compact surface, the electrolyte cannot enter the interior of the PPy, resulting in the decrease of specific capacitance. This result is in good agreement with the experimental result of the contact angle as shown in Fig. 4. The areal specific capacitance of the four samples increases when the Py concentration increases (Fig. 5e), because the mass of PPy covered on paper per unit area increased with the Py concentration increasing (Fig. 5f). Notably, as

shown in Fig. 5e, the specific capacitances or areal specific capacitances of the PPy/paper samples obtained by the CV curve decrease significantly with the increase of scan rate or the current density. The reason is that there is no enough time for the electrolyte to get access into the interior of the PPy coated on the cellulose fibers, and this limitation is particularly significant for the electrodes with thick polymer layers [31].

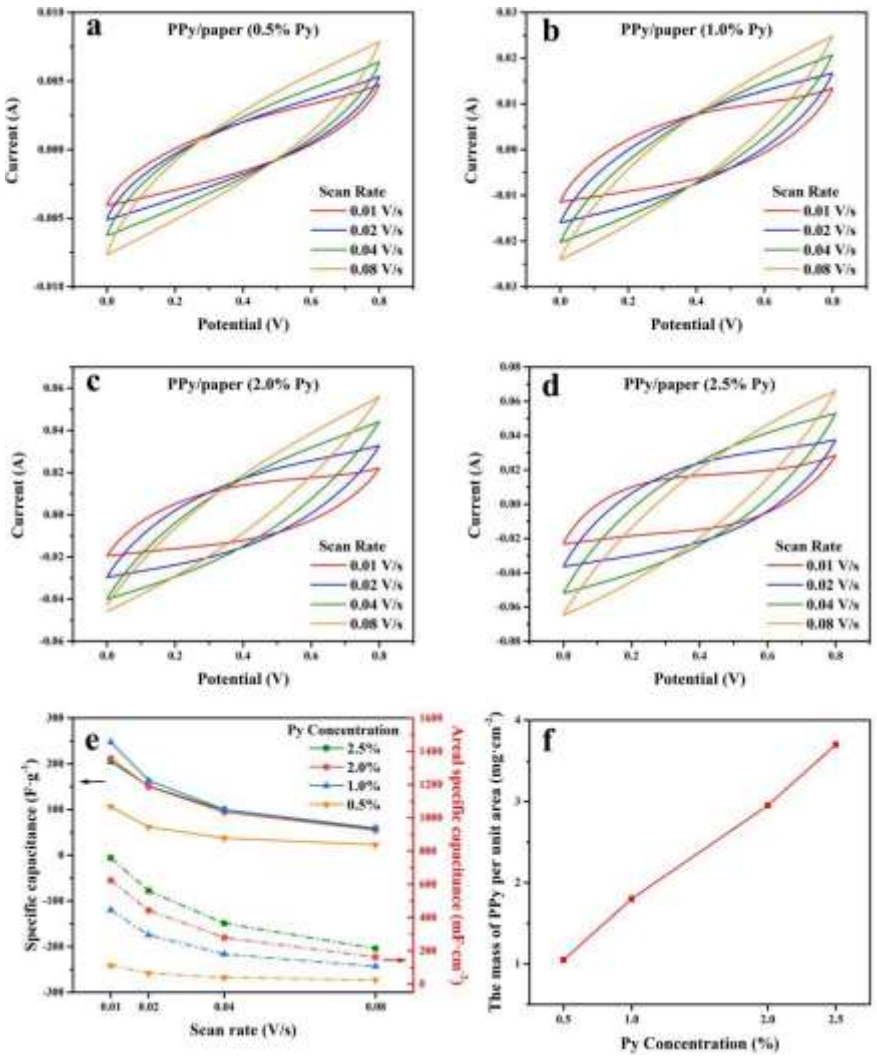

Fig. 5. (a-d) CV curves of PPy/paper samples fabricated with 0.5% (a), 1.0% (b), 2.0% (c), 2.5% (d) Py concentration at different scan rates; (e) The specific capacitance and the areal specific capacitance at different scan rates for four PPy/paper samples; (f) The mass of PPy per unit area on the electrodes fabricated with different Py concentration.

GCD measurements at different discharging currents and EIS were carried out to further investigate the electrochemical performance of PPy/paper electrodes. Fig. 6a-d exhibit the discharge part of the GCD curves of PPy/paper electrodes at different currents ranging from 4 mA to 10 mA. It can be seen that the discharge time of the four samples increases with the decrease of the Py concentration. Based on the above GCD curves, the corresponding specific capacitances and areal specific capacitances are calculated (Fig. 6e). The values of specific capacitances are about 66.7 F/g, 369.4 F/g, 336.0 F/g and 339.2 F/g for the PPy/paper samples at different Py concentrations of 0.5%, 1.0%, 2.0% and 2.5% at 4 mA. It is obvious that PPy/paper (1.0% Py) still maintains the highest specific capacitance among all the electrodes under different discharge currents, which is in accordance with the result obtained from CV curves (Fig. 5e). It can be found that specific capacitances and areal specific capacitances of the four samples decrease when the current increases from 4 mA to 10 mA. Furthermore, Fig. 6f shows the Nyquist plots of all samples at the frequency range of 0.01 Hz to 100 kHz with an AC perturbation of 5 mV. All the EIS are similar with a semicircle at high frequency region and a slope at low frequency. At high frequency, the intercept of curves on the real axis represents the equivalent series resistances (ESRs) of the PPy/paper electrodes, which are 10.5 Ω, 7.4 Ω, 4.8 Ω and 3.8 Ω for the PPy/paper samples at different Py concentrations of 0.5%, 1.0%, 2.0% and 2.5%, respectively. It can be seen that the values of ESRs for the PPy/paper electrodes fabricated with different Py concentrations decrease as the Py concentration increases from 0.5% to 2.5%, which could be ascribed to that the conductivity of PPy/paper became better when more and more PPy coated on the surface of cellulose paper under higher Py concentration. Moreover, in EIS spectra, the diameter of the semicircle in high frequency region refers to the charge transfer resistance (Rct). The values of the Rct are 12.7 Ω, 1.7 Ω, 1.2 Ω and 0.3 Ω for

the PPy/paper samples at different Py concentration of 0.5%, 1.0%, 2.0% and 2.5%, respectively. It is obvious that Rct values of the PPy/paper electrodes decrease dramatically as the Py concentration increases from 0.5% to 1.0%, and PPy/paper (2.5% Py) maintains the smallest Rct, which indicates a faster ionic transfer and electrochemical reaction [32]. Finally, PPy/paper (1.0% Py) was chose as the electrode to fabricate the solid-state paper-based supercapacitors because it possesses the best specific capacitance among all the samples.

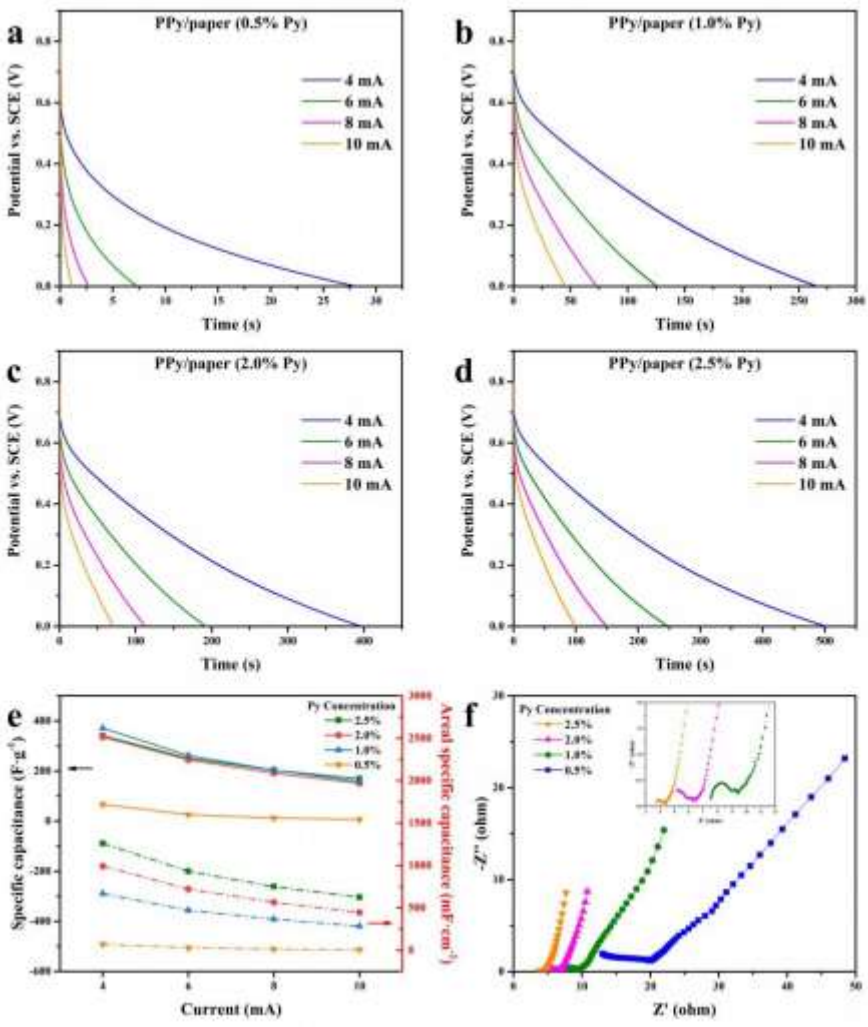

Fig. 6. (a-d) Discharge part of GCD curves of PPy/paper samples fabricated with 0.5% (a), 1.0% (b), 2.0% (c), 2.5% (d) Py concentration at different currents; (e) The specific capacitance and the areal specific capacitance at different currents of the PPy/paper samples; (f) EIS of the samples carried out in a frequency range of 0.01 Hz to 100 kHz.

Bending tests on the PPy/paper (1.0% Py) were conducted to illustrate its flexibility and the electrical stability. Fig. 7 shows the relative conductivity of the sample after different bending times. The sample had been bent in the same direction and the corresponding conductivity was recorded when the bending times reached 50, 150, 250, 350 and 450, respectively. It is obvious that the conductivity of the PPy/paper still retains near the original value after being bent 450 times. The inset in Fig. 7 shows a circuit formed by connecting the PPy/paper strip with a button battery which can light up a LED when the PPy/paper was folded and touched the metal electrode of the battery. The LED could be lit up even when the PPy/paper was bent at 180° after 450 times. This demonstrates that the PPy/paper has a superior stability of electrical conductivity and a very good flexibility. When PPy was coated on the cellulose fibers, the hydrogen bonds were formed between the N at the pyrrole rings and hydroxyl groups of cellulose fibers, resulting in a superior adhesion of PPy on paper, which is beneficial to the flexibility and stable conductivity [33].

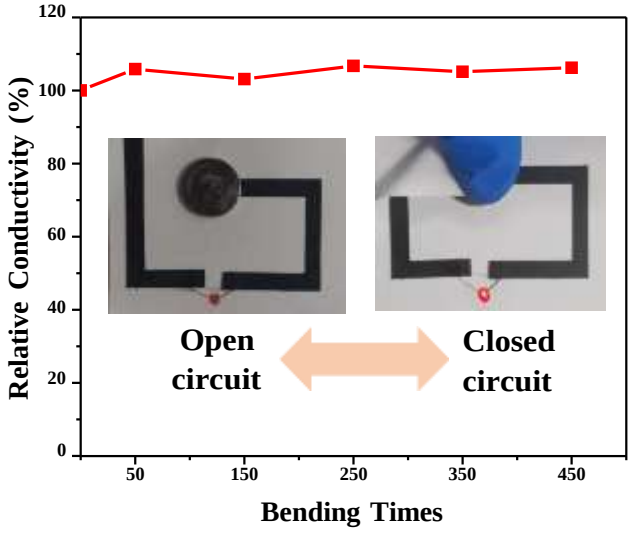

Fig. 7. Relative conductivity of the PPy/paper (1.0% Py) after different bending times. The inset shows the pictures of conducting circuit by folding the PPy/paper (1.0% Py) to light up the LED using a button battery as the power source.

Fig. 8 shows the electrochemical properties of the paper supercapacitors units fabricated. PPy/paper (1.0% Py) was cut by laser-cutting to obtain electrodes with matched structures, a solid-state paper-based supercapacitor unit (thickness, about 275 μm) was prepared by assembling two electrodes with matched structures and PVA/H_3PO_4 gel electrolyte together as shown in the inset of Fig. 8a. Three supercapacitor units were produced, marked as Sample 1, 2, and 3. The CV curves of the three supercapacitor units are displayed in Fig. 8a, which were tested within a potential range of 0-0.8 V at a scan rate of 0.01 V s^{-1}. The CV curves present similar shapes and the corresponding areal specific capacitances are 13.6 mF cm^{-2}, 13.7 mF cm^{-2} and 12.9 mF cm^{-2} for Sample 1, Sample 2 and Sample 3, respectively, indicating a high repeatability of fabrication and stability of electrochemical performance of the supercapacitors.

The CV curves of Sample 3 within a potential range of 0-0.8 V at different scan rates are plotted in Fig. 8c. With the scan rates increasing from 0.01 V s^{-1} to 0.08 V s^{-1}, the areal specific capacitance values decrease from 12.9 mF cm^{-2} to 2.8 mF cm^{-2} as shown in Fig. 8e (12.9 mF cm^{-2} at 0.01 V s^{-1}, 10.3 mF cm^{-2} at 0.02 V s^{-1}, 5.0 mF cm^{-2} at 0.04 V s^{-1} and 2.8 mF cm^{-2} at 0.08 V s^{-1}, respectively). Fig. 8d shows the GCD curves of Sample 3 at different currents ranging from 0.4 mA to 0.8 mA. There are relatively large IR drops for GCD curves, the possible reason is that the poor contact between PVA gel electrolytes and electrodes or slow ion transfer rate in gel electrolytes. As shown in Fig. 8e, the areal specific capacitances also decrease as the current increasing. The reason is that there is no enough time for the electrolyte to get access into the interior of PPy coated on the cellulose fibers. Fig. 8f shows the Nyquist plot at the frequency range of 0.01 Hz to 100 kHz with an AC perturbation of 5 mV. At high frequency, the intercepting point on the real axis represents the ESR of the device which is about 111

Ω. From the enlarged view of the high-frequency region in Fig. 8f, the curve shows a semicircle with a small diameter, indicating a low charge transfer resistance Rct (about 33 Ω). And the slope is near 45° in the low-frequency region, indicating the Warburg impedance related to the diffusion of electrolyte within the PPy on the cellulose fibers.

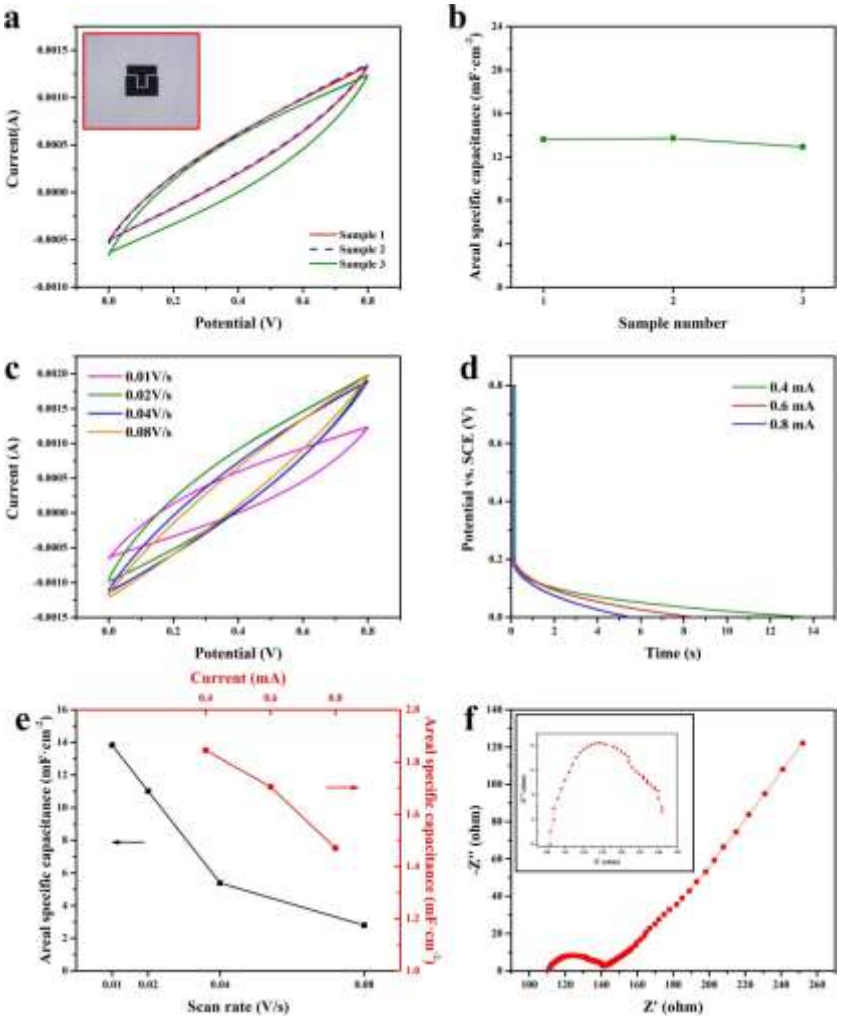

Fig. 8. (a) CV curves of Sample 1, 2 and 3 at a scan rate of 0.01 V s^{-1}; (b) The areal specific capacitance of three samples calculated based on CV curves (the inset shows the picture of paper-based supercapacitor unit); (c) CV curves of Sample 3 at different scan rates; (d) Discharge part of GCD curves for Sample 3 at different currents; (e) The areal specific capacitance of Sample 3 calculated based on CV curves and GCD curves, respectively; (f) The Nyquist plots of Sample 3 recorded in a frequency range from 0.01 Hz to 100 kHz (the inset shows the enlarged view of the high-frequency region).

The C_A and E_A values of solid-state paper-based supercapacitor in this work have been compared with the solid-state paper-based supercapacitors reported previously. The device prepared in this work maintains a relatively satisfactory capacitive property, its areal specific capacitance (12.9 mF cm^{-2}) is higher compared with some reported paper-based supercapacitors, such as CNFs/$[RGO]_{20}$ hybrid paper (0.78 mF cm^{-2} at a scan rate of 0.005 V s^{-1}) [8], Mo_3C_2-graphene composite paper (9.5 mF cm^{-2} at a scan rate of 0.01 V s^{-1}) [34], 3D-graphene coated graphite-paper (11.1 mF cm^{-2} at a scan rate of 0.005 V s^{-1}) [35]. The highest energy density of 1.15 μWh cm^{-2} for paper-based supercapacitor obtained at a scan rate of 0.01 V s^{-1} is comparable with that for the device using 3D-graphene coated graphite-paper electrode (1.24 μWh cm^{-2}) in ref [35]. This advantage could be ascribed to the better conductivity, hydrophilicity and porous structure of the PPy/paper.

To demonstrate the performance of the devices in practical application, the fabricated supercapacitor units were connected in series and/or parallel to improve their operating voltage and current. Fig. 9a shows the photo of three energy storage groups. In the left part of the photo, two supercapacitor units (Sample 1 and Sample 2) were connected in series (denoted as Series) or in parallel (marked as Parallel). In the right part of the photo, the device consists four supercapacitor units, in which every two supercapacitor units were first connected in series and then in parallel (marked as Series & Parallel). Fig. 9b exhibits the CV curves of Sample 1, Sample 2 and devices connected in different types at a scan rate of 0.01 V s^{-1}. The capacitances based on CV curves were calculated and listed in Table 1. It could be seen that CV curves of Sample 1 and Sample 2 are almost the same, and the corresponding capacitance for Sample 1 and Sample 2 are 54.4 mF and 54.8 mF, respectively, indicating their similar electrochemical properties and good repeatability. When the two prepared supercapacitor units were connected in

series, two times enhanced potential window could be provided. It is also worth noting here that the measured capacitance of Series is 42.6 mF, which was is 56.0% higher than the theoretical value (27.3 mF). Two supercapacitor units in series were directly assembled with the electrodes prepared by laser-cutting, instead of connecting two fabricated supercapacitors together with wires, this might reduce the internal resistance to obtain a better capacitance. When two supercapacitor units were connected in parallel, the capacitance value reaches 126.8 mF, which is also 15% higher than the theoretical (109.2 mF). In Series & Parallel connection, the total capacitance was 81.4 mF, which is higher than the theoretical capacitance calculated based on Sample 1 and Sample 2 (54.6 mF), while it is very close to the value that two Series samples were connected in parallel (85.2 mF).

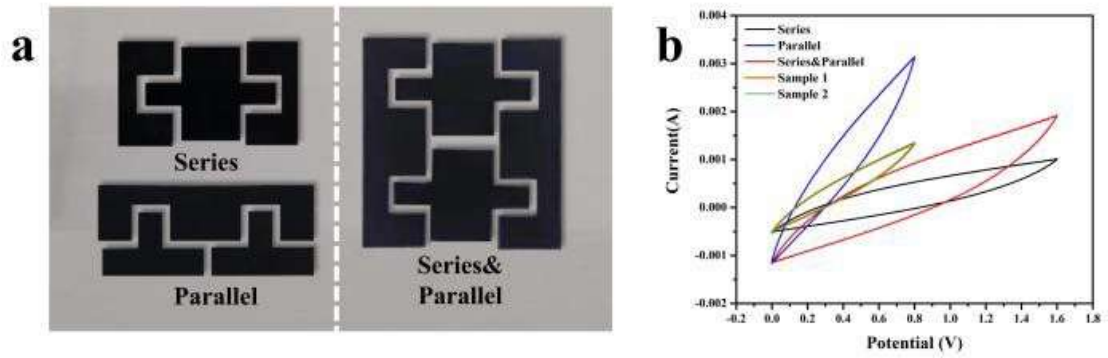

Fig. 9. (a) Optical picture of the fabricated supercapacitors in different connections; (b) CV curves of supercapacitors in different connections, Sample 1 and Sample 2 at a scan rate of 0.01 V s^{-1}.

Table 1. Comparison of the measured values and theoretical values of Sample 1, Sample 2 and the devices fabricated with different connection types at a scan rate of 0.01 V s^{-1}.

	Scan rate ($V\ s^{-1}$)	Capacitance (mF)	Theoretical value (mF)
Sample 1	0.01	54.4	
Sample 2	0.01	54.8	
Series	0.01	42.6	27.3
Parallel	0.01	126.8	109.2
Series& Parallel	0.01	81.4	54.6

In consideration of solid-state paper-based supercapacitors fabricated for practical use, a FPCB was designed and constructed with three small LEDs in parallel, a current limiting resistor, the charging interfaces and two switches. And a solid-state paper-based supercapacitors array was assembled by eight fabricated supercapacitor units, in which four supercapacitor units were in series and then in parallel connection (Fig. 10a). Then, the above mentioned components and solid-state paper based supercapacitors group were integrated on the front of a FPCB (Fig. 10b) according to the equivalent circuit diagram shown in the inset of Fig. 10d. Fig. 10c shows that the supercapacitor array was adhered to the back of FPCB. The supercapacitor array was connected to the circuit by linking the copper wires on the front and the two copper conductive tapes on the back together. The thickness of the supercapacitor array was very small, which can be seen from the lateral view of the device, Fig. 10e. The thin paper-based supercapacitor array fabricated was easy to integrated with FPCB, and the charged

paper-based supercapacitors array could light up 3 red LEDs even under a bent state, exhibiting its good flexibility, Fig. 10f. These solid-state paper-based supercapacitor units, which are thinner, uniform and can be assembled to obtain flexible devices with different voltage and current, are easily integrated with FPCB, reflecting the possibility of its potential broad applications in portable/wearable electronics as an energy storage device.

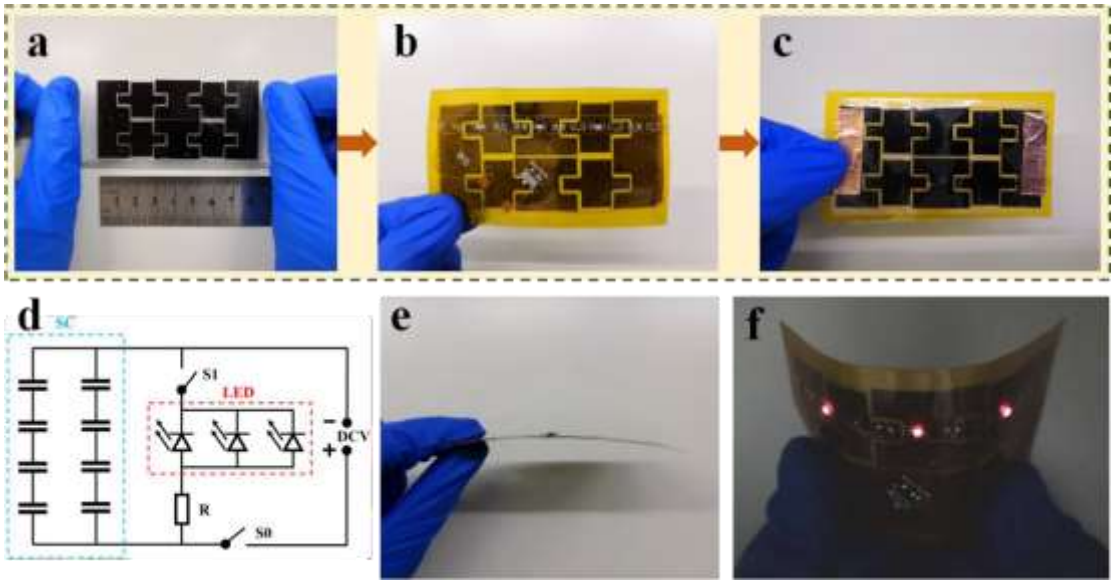

Fig. 10. (a) The photo of the supercapacitors array assembled by supercapacitor units in series and parallel connection; (b) The photo of the front of FPCB, exhibiting the integration of three parallel LEDs, current limiting resistor, charging interfaces, copper wires and two switches on FPCB after supercapacitors adhered to the back of FPCB; (c) The photo of the back of FPCB, showing the assembled supercapacitors and two copper plate lugs; (d) Schematic of the circuit design on FPCB; (e) The lateral view of the assembled device demonstrating its thin thickness; (f) Image of the working device in bending state.

4 Conclusion

In summary, conductive PPy/paper electrodes were prepared by a chemical interfacial polymerization method using cellulose paper as the flexible substrate. Among all the PPy/paper samples prepared with different Py concentration of 0.5%, 1.0%, 2.0% and 2.5%, PPy/paper (1.0% Py) shows excellent electrochemical performance (445.3 mF cm^{-2} and 247.4 F/g at 0.01 V s^{-1}), and a good flexibility: the conductivity of PPy/paper (1.0% Py) could retain near the original value even after bending 450 times. Then the PPy/paper (1.0% Py) electrodes with matched shapes were prepared accurately and easily by laser cutting. Furthermore, a planar solid-state supercapacitor unit has been fabricated using the PPy/paper electrodes and it shows a high areal specific capacitance of 12.9 mF cm^{-2}, an excellent rate performance and an outstanding energy density of 1.15 μW h cm^{-2} at a scan rate of 10 mV s^{-1}. In addition, several supercapacitor units can be assembled like Lego in parallel or in series to meet the voltage and energy requirements. The assembled supercapacitor array consisting 8 supercapacitor units was integrated with a FPCB and lighted up 3 LEDs, even under bending conditions. Overall, this work offers an effective approach to fabricate flexible paper-based solid-state planar supercapacitors to power various portable and wearable electronics.

Acknowledgements

This work was supported by National Natural Science Foundation of China (51905445), Natural Science Foundation of Shaanxi Province (2018JQ5020) and Fundamental Research Funds for the Central Universities (31020190503005).

References:

[1] Wong W-S, Salleo A. Flexible electronics. Science 2009;11(323):1566-7.

[2] Nyholm L, Nyström G, Mihranyan A, Strømme M. Toward flexible polymer and paper-based energy storage devices. Adv Mater 2011;23(33):3751-69.

[3] Wang X, Lu X, Liu B, Chen D, Tong Y, Shen G. Flexible energy-storage device: design consideration and recent progress. Adv Mater 2014;26(28):4763-82.

[4] Miao F, Shao C, Li X, Lu N, Wang K, Zhang X, Liu Y. Polyaniline-coated electrospun carbon nanofibers with high mass loading and enhanced capacitive performance as freestanding electrodes for flexible solid-state supercapacitors. Energy 2016;95:233-41.

[5] El-Kady M-F, Strong V, Dubin S, Kaner R-B. Laser scribing of high-performance and flexible graphene-based electrochemical capacitors. Science 2012;335(6074): 1326-30.

[6] Xia L, Li X, Wu Y, Hu S, Liao Y, Huang L, Qing Y, Lu X. Electrodes derived from carbon fiber-reinforced cellulose nanofiber/multiwalled carbon nanotube hybrid aerogels for high-energy flexible asymmetric supercapacitors. Chem Eng J 2020;379:122325.

[7] Jiang Z, Zhai S, Huang M, Songsiriritthigul P, Aung S-H, Oo T-Z, Luo M, Chen F. 3D carbon nanocones/metallic MoS_2 nanosheet electrodes towards flexible supercapacitors for wearable electronics. Energy 2021;227:120419.

[8] Gao K, Shao Z, Wu X, Wang X, Zhang Y, Wang W, Wang F. Paper-based transparent flexible thin film supercapacitors. Nanoscale 2013;5(12):5307-11.

[9] Ko Y, Kwon M, Bae W-K, Lee B, Lee S-W, Cho J. Flexible supercapacitor electrodes based on real metal-like cellulose papers. Nat Commun 2017;8(1):536.

[10] Zhang Y-Z, Wang Y, Cheng T, Lai W-Y, Pang H, Huang W. Flexible supercapacitors based on paper substrates: a new paradigm for low-cost energy storage. Chem Soc Rev 2015;44(15):5181-99.

[11] Feng J-X, Li Q, Lu X-F, Tong Y-X, Li G-R. Flexible symmetrical planar supercapacitors based on multi-layered MnO_2/Ni/graphite/paper electrodes with high-efficient electrochemical energy storage. J Mater Chem A 2014;2(9):2985-92.

[12] Yao B, Zhang J, Kou T, Song Y, Liu T, Li Y. Paper‐Based Electrodes for Flexible Energy Storage Devices. Adv Sci 2017;4(7):1700107.

[13] Zheng G, Hu L, Wu H, Xie X, Cui Y. Paper supercapacitors by a solvent-free drawing method. Energy Environ Sci 2011;4(9):3368-73.

[14] Down M-P, Foster C-W, Ji X, Banks C-E. Pencil drawn paper based supercapacitors. RSC Adv 2016;6(84):81130-41.

[15] Yang P, Mai W. Flexible solid-state electrochemical supercapacitors. Nano Energy 2014;8:274-90.

[16] Niu Z, Zhang L, Liu L, Zhu B, Dong H, Chen X. All-solid-state flexible ultrathin micro-supercapacitors based on graphene. Adv Mater 2013;25(29):4035-42.

[17] Tong L, Gao M, Jiang C, Cai K. Ultra-high performance and flexible polypyrrole coated CNT paper electrodes for all-solid-state supercapacitors. J Mater Chem A 2019;7(17):10751-60.

[18] Wang Y, Shi Y, Zhao C-X, Wong J-I, Sun X-W, Yang H-Y. Printed all-solid flexible microsupercapacitors: towards the general route for high energy storage devices. Nanotechnology 2014;25(9):0941010.

[19] Yu Y, Zhang J. Pencil-drawing assembly to prepare graphite/MWNT hybrids for high performance integrated paper supercapacitors. J Mater Chem A 2017;5(9):4719-25.

[20] Snook G-A, Kao P, Best A-S. Conducting-polymer-based supercapacitor devices and electrodes. J Power Sources 2011;196(1):1-12.

[21] Qian W, Gao Q, Zhang H, Tian W, Li Z, Tan Y. Crosslinked polypyrrole grafted Reduced grapheme oxide-sulfur nanocomposite cathode for High performance Li-S Battery. Electrochim Acta 2017;235:32-41.

[22] Chen Y, Cai K, Liu C, Song H, Yang X. High-Performance and Breathable Polypyrrole Coated Air-Laid Paper for Flexible All-Solid-State Supercapacitors. Adv Energy Mater 2017;7(21):1701247.

[23] Fu L, Fu X, Zhao G. Laser Carving Assisted Preparation of Polypyrrole Coated Paper-Based Supercapacitors. Chem Phys Lett 2021;765:138290.

[24] Spicar-Mihalic P, Toley B, Houghtaling J, Liang T, Yager P, Fu E. CO_2 laser cutting and ablative etching for the fabrication of paper-based devices. J Micromech Microeng 2013;23:067003.

[25] Chen X, Qian X, An X. Using calcium carbonate whiskers as papermaking filler. BioResources 2011;6(3):2435-47.

[26] Yuan L, Yao B, Hu B, Huo K, Chen W. Polypyrrole-coated paper for flexible solid-state energy storage. Energy Environ Sci 2013;6(4):470-6.

[27] Li X-G, Li A, Huang M-R, Liao Y, Lu Y-G. Efficient and Scalable Synthesis of Pure Polypyrrole Nanoparticles Applicable for Advanced Nanocomposites and Carbon Nanoparticles. J Phys Chem C 2010;114(45):19244-55.

[28] Qu L, Shi G, Chen F, Zhang J. Electrochemical Growth of Polypyrrole Microcontainers. Macromolecules 2003;36(4):1063-7.

[29] Zang J, Li C, Bao S, Cui X, Bao Q, Sun C. Template-Free Electrochemical Synthesis of Superhydrophilic Polypyrrole Nanofiber Network. Macromolecules 2008;41(19):7053-7.

[30] Zhang D, Qiu S, Huang W, Yang D, Wang H, Fang Z. Mechanically strong and electrically stable polypyrrole paper using high molecular weight sulfonated alkaline lignin as a dispersant and dopant. J Colloid Interface Sci 2019;556:47-53.

[31] Snook G-A, Peng C, Fray D-J, Chen G-Z. Achieving high electrode specific capacitance with materials of low mass specific capacitance: potentiostatically grown thick micro-nanoporous PEDOT films. Electrochem Commun 2007;9(1):83-8.

[32] Song Y, Xu J-L, Liu X-X. Electrochemical anchoring of dual doping polypyrrole on graphene sheets partially exfoliated from graphite foil for high-performance supercapacitor electrode. J Power Sources 2014;249:48-58.

[33] David N-C, Anavi D, Milanovich M, Popowski Y, Frid L, Amir E. Preparation and properties of electro-conductive fabrics based on polypyrrole: covalent vs. non-covalent attachment. IOP Conf Ser: Mater Sci Eng 2017;254(3):032002.

[34] Zang X, Shen C, Chu Y, Li B, Wei M, Zhong J, Sanghadasa M, Lin L. Laser-Induced Molybdenum Carbide-Graphene Composites for 3D Foldable Paper Electronics. Adv Mater 2018;30(26):1800062.

[35] Ramadoss A, Yoon K-Y, Kwak M-J, Kim S-I, Ryu S-T, Jang J-H. Fully flexible, lightweight, high performance all-solid-state supercapacitor based on 3-Dimensional-graphene/graphite -paper. J Power Sources 2017;337:159-65.

Declaration of interests

☒The authors declare that they have no known competing financial interests or personal relationships that could have appeared to influence the work reported in this paper.

☐The authors declare the following financial interests/personal relationships which may be considered as potential competing interests: